THE JOURNAL OF PHYSICAL CHEMISTRY C

Article

pubs.acs.org/JPCC

Gold-Induced Unfolding of Lysozyme: Toward the Formation of Luminescent Clusters

Debasmita Ghosh,[†,‡] Ananya Baksi,[†,‡,§] Sathish Kumar Mudedla,[∥] Abhijit Nag,[†] Mohd Azhardin Ganayee,[†] Venkatesan Subramanian,[∥] and Thalappil Pradeep*[,†]

[†]DST Unit of Nanoscience (DST UNS) & Thematic Unit of Excellence (TUE), Department of Chemistry, Indian Institute of Technology Madras, Chennai-600036, India

[∥]Chemical Laboratory, CSIR-Central Leather Research Institute, Adyar, Chennai-600020, India

Supporting Information

ABSTRACT: Ion mobility mass spectrometry studies on Au_n-Lyz adducts showed gradual unfolding of the protein structure during binding of Au^+ to the protein. The change of the charge state envelope in Au_n-Lyz from that of Lyz in ESI MS data confirmed the relaxation of the protein structure. This Au^+ binding occurs at cysteine sites through the breakage of disulfide bonds and this ruptures the H-bonded folded network structure of the protein leading to ∼30% change in helicity. Nearly 15% loss in the total H-bonding occurred during the attachment of 8 Au to the protein as calculated by a molecular dynamics simulation. Different Au_n-Lyz structures were simulated, which confirmed significant unfolding of the protein. The structural insights were used to understand similar unfolding in the solution state as seen via circular dichroism (CD) and Fourier transform infrared (FTIR) spectroscopy. This open structure is indeed necessary to accommodate a cluster core inside a protein cavity during luminescent cluster synthesis. These studies unambiguously establish noble metal binding-induced conformational changes of protein structures to accommodate the clusters.

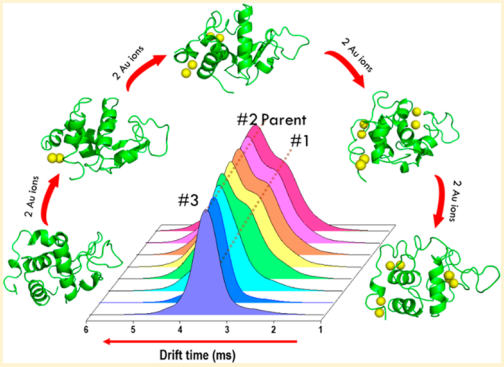

INTRODUCTION

Atomically precise, luminescent clusters of noble metals, especially gold, are new materials of immense promise.[1−6] Intense luminescence, molecular nature of subnanometer dimensions, possibility to incorporate in various matrices,[7−9] novel catalysis,[10] and efficient sensing of analytes[11,12] are some of the important benefits of such cluster materials. While research in this area has expanded tremendously in the recent past, another fascinating area has emerged in which metal clusters are grown in protein templates. Metal nanoparticles have been grown in Lysozyme crystals.[13−17] These clusters embedded in proteins have been characterized extensively with mass spectrometry (MS).[18−22] However, their structures have not been precisely determined by X-ray diffraction (XRD). Even with this limitation, this area of protein protected clusters has grown rapidly due to the stability of their luminescence,[23−26] especially in chemical and biological situations. An important application area of such luminescent clusters is in sensing of metal ions and organic analytes. The luminescence property has been used widely for sensing of heavy metal ion[11,12,17,27] in water and for small molecules of biological relevance.

Development of reliable, sensitive, and biocompatible platforms are highly desirable in modern biomedical research.[28] Surface functionalization of NCs with protein, peptide, and DNA make them biocompatible, which allows them to be used for biomedical applications[29] for special binding and targeted drug delivery,[30,31] multimodal imaging,[32−34] therapeutic applications,[35] targeted biolabeling,[36−38] and so on.

Despite the large interest in such materials, their formation and associated effects have not been explored in detail. In a recent report, Baksi et al. looked at the growth of clusters in lysozyme (Lyz) and bovine serum albumin (BSA) in solution using small-angle X-ray scattering (SAXS) and found that during the formation of clusters, the protein size changes significantly, leading to a higher degree of unfolding.[39] In a typical cluster synthesis, metal ion (specifically gold) at an appropriate concentration is complexed with the protein (∼pH 5.5), which is known as the adduct. The metal-protein adduct is subjected to reduction in highly basic conditions, typically using NaOH. While the protein and the adduct at pH 5.5 can be examined in electrospray ionization mass spectrometry (ESI MS), the cluster formed in basic condition (pH 12) does not ionize effectively by ESI MS. As a result, no ESI MS of protein bound clusters is known until now. All such studies of clusters have been confined through matrix-assisted laser desorption ionization (MALDI) MS.

While these equilibrium studies examined protein shell and the cluster core in some detail, the early stages of cluster formation, namely, the metal ion protein adducts have not been

Received: March 15, 2017
Revised: May 31, 2017
Published: May 31, 2017

DOI: 10.1021/acs.jpcc.7b02436
J. Phys. Chem. C 2017, 121, 13335−13344

looked at in detail in any of the reports. Proteins are known to form adducts with metals, especially at the carboxylate ends. Such noncovalent interactions, also known as nonspecific binding, leads to contraction of the protein as a whole.[40−42] Such investigations of noncovalent protein binding with metal ions and corresponding structural changes have been explored through ion mobility mass spectrometry. On the other hand, interactions of the noble metal with protein is supposed to be specific (covalent), expected to happen through the cysteine sites. Moreover, such studies performed on adducts of relevance to protein protected clusters is expected to derive new insights into the early stages of cluster formation.

In the following, we present an investigation of the Au_n-Lyz system just after the addition of Au ions into the protein when the pH is 5.5. Using ion mobility along with ESI MS, our studies have shown distinct Au_n-Lyz (n = 1−8) species, all of which exhibit different conformers. An analysis of the Au_n-Lyz species established the gradual opening of the protein structure with increasing n, allowing the accommodation of the cluster core inside. A computational analysis of the gradual structural relaxation shows a significant unfolding of the protein, a large change in its secondary structure upon binding with Au in solution. Breakage of disulfide bonds, as well as a decrease in H-bonding, are directly related to the unfolded state of the protein. Calculated structural change is in good agreement with the collision cross section (CCS) values determined from ion mobility studies. Experimental studies show that structural relaxation occurs, in the solution state itself. Here, for the first time, we have shown how a noble metal ion can affect the protein structure in the process of cluster formation.

EXPERIMENTAL SECTION

Reagents and Materials. Tetrachloroauric acid trihydrate ($HAuCl_4{\cdot}3H_2O$) was prepared in-house starting from elemental gold. Lyz (>90% purity) was purchased from Sigma-Aldrich. Millipore water was used in all the experiments.

Instrumentation. All the experiments described in this paper were carried out using a Waters Synapt G2Si HDMS instrument. The instrument consists of an electrospray source, quadrupole ion guide/trap, ion mobility cell, and TOF detector. Different gases were used in different parts of the instrument. Nitrogen was used as the nebulizer gas. Ultrahigh pure N_2 (99.9995%) was used inside the ion mobility cell and the ions were directed through a drift tube. To reduce fragmentation, helium was used as the curtain gas (ion cooling) before the ions entered the mobility cell. High pure Ar gas was used for collision induced dissociation (CID). All the experiments were done in positive ion mode.

To get the well-resolved mass spectrum in ion mobility (ESI IM-MS) mode, the following instrumental parameters were used: sample concentration, 1 μg/mL; solvent, water; flow rate, 10−20 μL/min; capillary voltage, 2−3 kV; cone voltage, 65 V; source offset, 0 V; desolvation gas flow, 400 L/h; trap gas flow, 1.5 mL/min; He gas flow, 90 mL/min; ion mobility gas flow, 25 mL/min; bias voltage, 45 V; wave velocity, 500 m/s; wave height, 15 V.

For probe distance dependent study, the distance of the probe from the MS inlet was gradually changed from 5 to 10 mm and IMS was collected at those distinct spray positions.

Fourier transform infrared (FTIR) spectra were measured with a PerkinElmer Spectrum One instrument. KBr crystals were used as the matrix for preparing the samples. The second derivative of FTIR spectrum was taken using "spectrum one" software provided by PerkinElmer.

Circular dichroism (CD) spectra were measured in a Jasco 815 spectropolarimeter with Peltier setup for the temperature-dependent measurements. CD studies were done with a 10 mm path length cell. The concentration of the sample in the cuvette used for CD measurement was 2×10^{-6} g mL^{-1}.

Synthesis. Lyz (150 μM) and Au^{3+} were incubated at different molar ratios such as 1:1.5, 1:3 and 1:4 (Lyz/Au^{3+}) for 3 h. In the case of 1:4 ratio, attachment of seven Au ions was observed. Before ESI MS and Ion Mobility MS study, these adducts were diluted with Millipore water.

Computational Details. The structure of Lyz was taken from protein data bank (pdb id: 1AKI).[43] The structure of Lyz at pH 5.5 and 7 are shown in Figure S1. Molecular dynamics (MD) simulations have been performed for the structure of Lyz in which the amino acids (Asp, Glu, and His) were protonated. The structure at the end of the simulation (at 100 ns) was considered to bind with gold ions. The cysteine (CYS) residues involved in disulfide bonds were changed to deprotonated cysteine (CYM) with −1 charge. Then Au^+ were covalently attached to the sulfur of CYM. AMBER99 force field was used for Lyz.[44] Lennard-Jones parameters for gold atoms were obtained from the literature and the charge used for gold atoms was +1.[45,46] The force constants for bonds and angles that involved gold atoms were taken from previous reports.[45,46] The structures of Lyz with gold ions were solvated in a cubic box using the TIP3P model. The positive charge of Lyz was neutralized by adding Cl^- ions and those systems were energy minimized with the help of steepest decent method. The obtained structures were equilibrated for 1 ns at 300 K and 1 bar. Temperature and pressure were controlled using V-rescale and Parrinello−Rahman algorithms.[47−49] MD simulations have been performed for 100 ns using a time step of 2 fs with the help of Gromacs-4.6.2 package[50−52] in NPT ensemble. The electrostatic interactions were calculated using Particle Mesh Ewald with the interpolation order of 4 and a grid spacing of 1.6 Å.[53] Bonds between hydrogen and heavy atoms were constrained at equilibrium bond lengths using the LINCS algorithm.[54] The trajectories obtained from MD simulation were visualized using VMD.[55] The trajectories were analyzed using tools available in Gromacs package.

RESULTS AND DISCUSSION

In the course of cluster formation, the first step is the formation of metal-protein adducts (Au_n-Lyz), which was achieved by incubating the metal ions with the desired protein in solution. The covalent interaction between the noble metal ions and the protein leads to the formation of Au_n-Lyz and these are considered to be the intermediates for the protein protected clusters (Au@Lyz). To explore the Au_n-Lyz in the solution, we have performed an ESI MS study. Typical ESI MS obtained from any protein shows well-defined charge state distribution and is often used as a fingerprint for a specific protein. More folded or unfolded state of the same protein shows a different envelope. Shifting of the envelope toward higher charge state (lower m/z) is conventionally attributed to the unfolded state of the protein while shifting toward lower charge state (higher m/z) is considered to be due to more folded state of the same protein. Here as Lyz was studied in detail along with its gold bound adduct, definite changes in the distribution of the charge states were observed. In Figure 1, different charge states like $[M + 8H]^{8+}$, $[M + 9H]^{9+}$, $[M + 10H]^{10+}$, $[M + 11H]^{11+}$, and [M +

DOI: 10.1021/acs.jpcc.7b02436
J. Phys. Chem. C 2017, 121, 13335−13344

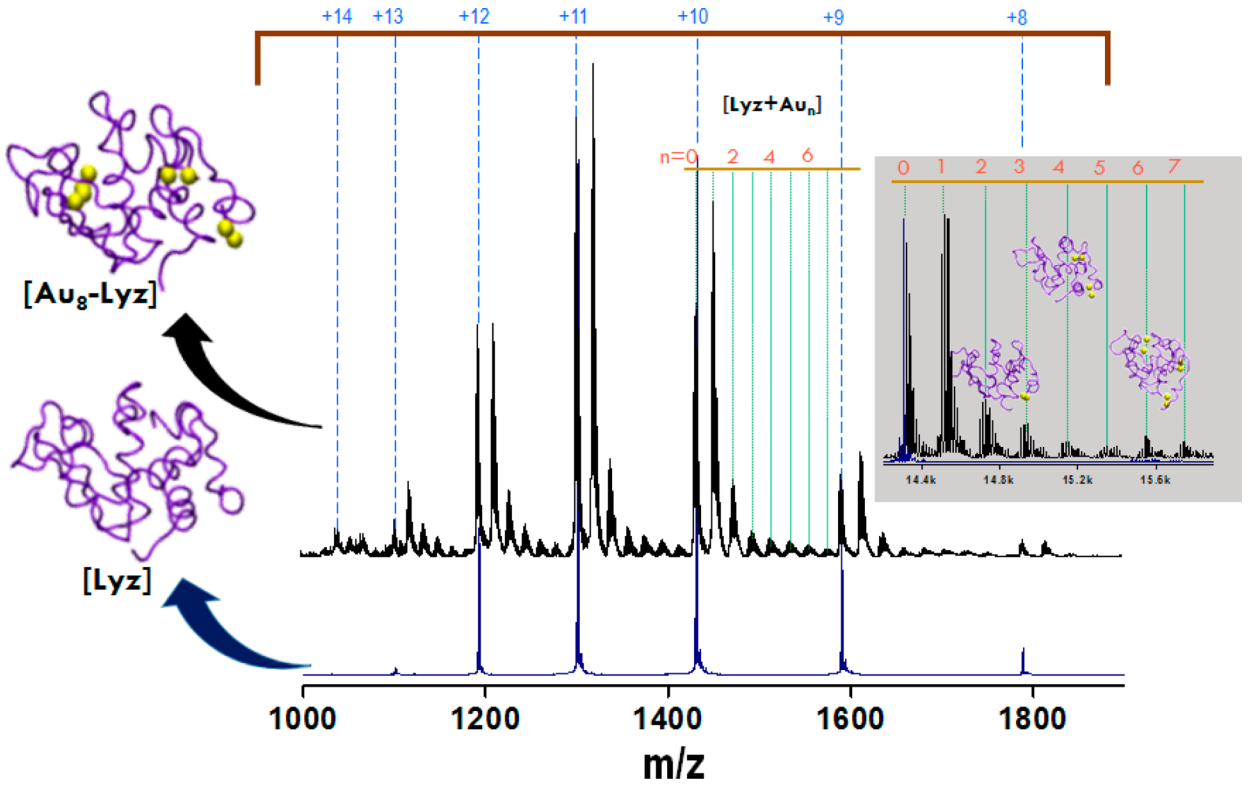

Figure 1. Comparative ESI MS of Lyz (blue) and Au bound Lyz (black) in positive mode, showing 7 Au attachments to a protein molecule. Deconvoluted spectrum achieved from the charge state and m/z distribution also shows seven Au attachments (inset). Schematics of protein and gold adducts are given.

12H]$^{12+}$ were observed, where M is the molecular ion of the protein. Charges lower than +8 were not seen for Lyz under these experimental and instrumental conditions, but using buffer solutions lower charge states like +7 or +6 have been observed for Lyz.[56]

The mass spectrum of the Lyz (blue trace) was compared with the Au$_n$-Lyz (black trace) in Figure 1, where +11 charge state appeared at maximum intensity, unlike the parent protein, which appeared at +10 charge state pointing toward the unfolded state of the protein due to metal attachment. Multiple Au attached peaks were observed. For low charge state, like +10 (m/z 1431), seven additional major peaks were observed separated by m/z 19.7 due to seven Au attachments. While the charge increased (lower m/z and lower separation between two neighboring charge states), up to five Au additions could be observed clearly for +12 and +13 charge states. The separation in the mass spectrum between the free protein peak and the gold uptake peaks changes with the charge state. The separation is 19.7 for +10 charge, while it is 21.9 for +9 and 24.6 for +8. The resulting full range MS was deconvoluted to achieve the molecular ion peak, which also confirmed seven Au attachment to the protein (inset of Figure 1). The separation of 197 in the deconvoluted mass spectrum indicates the attachment of one Au atom. Other peaks in a given cluster are due to the Na attachment and water attachment/detachment to/from the protein. Schematic of Au$_n$-Lyz are shown along with the corresponding spectrum. Crystal structure of Lyz was used for the construction of the schematic.

The protein, Lyz, has 129 amino acids, including eight cysteine [$SCH_2CH(NH_2)CO_2H$] residues and can form four disulfide bonds, located between positions 6 and 127, 30 and 115, 64 and 80, and 76 and 94. As shown later in the manuscript, theoretical simulations predicted that a maximum of eight Au ions can be attached to a single Lyz molecule. In the mass spectrum, however, up to seven Au attachments could be clearly observed (indicated in Figure 1). The peak corresponding to the eighth Au attachment merged with the next charge state of the Au$_n$-Lyz complex and, hence, was difficult to isolate in the MS. This is true for all the charge states. The appearance of higher charge states like +13 and +14 in the mass spectrum, and change in the charge state distribution was the indication of unfolding of the protein upon attachment of gold ions.[57]

Ion mobility is considered to add a third dimension to mass spectrometry, with the other two being intensity and the m/z value. Ion mobility coupled with ESI MS can measure the mass of a protein as well as can separate different conformers.[58,59] It is an easy way to separate isomers and is often considered as a gas phase chromatographic technique. As the name implies, the technique relies on the mobility of the ion in the gas phase, which strongly depends on its size and shape. Depending on the effective collision cross section (CCS, discussed later), different structural isomers can be separated along the time axis, often known as drift time. Drift time is directly proportional to m/z and the size of the molecule of interest. Considering proteins as the molecules of interest, different conformers will have different drift times, although they have the same m/z. When a protein molecule interacts with another entity and becomes unfolded or more folded in the process, changes in the drift time will give a direct proof of such changes in protein structure in the gas phase.

To incorporate the Au ion in Lyz, the disulfides bonds should break leading to a relatively opened structure. At the same time, H-bond forming amino acids will be separated, and hence, more unfolding will occur. This unfolding of the protein

DOI: 10.1021/acs.jpcc.7b02436
J. Phys. Chem. C 2017, 121, 13335−13344

structure will be reflected in the drift time and there will be a change in the relative population of the conformers. A detail IM-MS was performed to understand the structural change of the Lyz before Au@Lyz formation, in the gas phase. All the experimental conditions were kept the same for the next set of experiments. First full range ESI IM-MS were obtained and each of the peaks was studied for their respective drift time values. For convenience, only +10 charge state of different Au-attached Lyz peak was expanded in Figure 2. Parent Lyz had

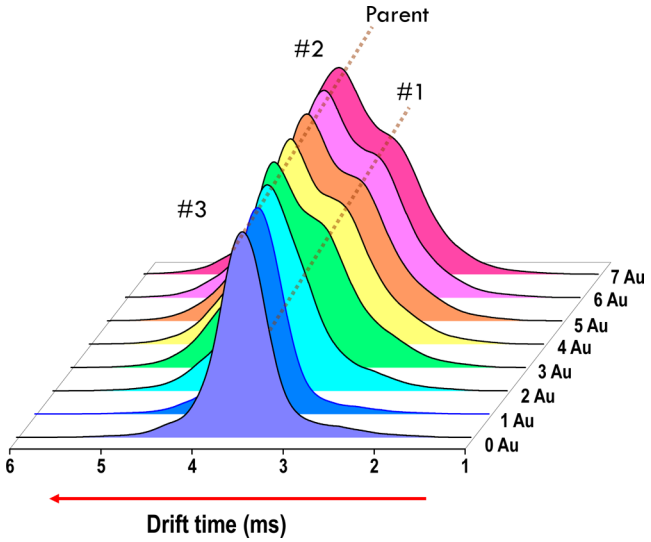

Figure 2. Ion mobility drift time of each Au-attached protein (for charge state +10) showing successive unfolding due to Au attachments. Broadening of the peaks signifies unfolding. Another hump at lower drift time suggests the opening of the protein to give an uncoiled conformer.

mostly one conformer at +10 charge state with mild interference of two other conformers and the peak for parent Lyz followed an almost Gaussian nature. The peak starts flattening at both ends with the emergence of two more peaks at either side of the main peak with increasing number of Au attachment to the protein.

Considering successive Au attachment to Lyz, the protein has to expand to accommodate multiple Au ions inside its cavity resulting more uncoiled structures leading to unfolding. These unfolded states will have their own conformers making it difficult to separate them from a broader envelope. An increase in protein size was reflected in the higher drift time of the conformer as seen in the mobilogram (Figure 2). This unwrapped structures of the Au_n-Lyz complexes lead to the higher drift time as a result of larger CCS. Slight shift at higher drift time may be a contribution of additional mass due to Au attachment. To disprove this possibility, we have done collision-induced unfolding (CIU) experiments, which will be discussed later in the manuscript (Figure 4).

In protein structure, majorly three conformers are present: folded, partially folded, and unfolded. Among these three conformers, the most abundant one having more uniform shape is attributed to the folded conformer. Here the conformers were denoted by #1, #2, and #3. After addition of Au ion to the protein, the parent conformer was named as #2 and, between the other two, #2 is partially folded. The conformer, which contributed to the broadened Gaussian shape of the parent conformer and almost nonseparable was #3, the unfolded one. The #1 conformer appeared at lower drift time, formed due to the phenomenon that, while the protein gets opened, some lower collision cross section species have been generated. This lower drift time conformer can be justified in another way. Considering elongation of the protein in one dimension, it is no more a spherical entity and hence have two axes with different length. In our experiment, drift time was calculated assuming a spherical approximation for the protein, which is no longer the case for its unfolded state. This can result in lower drift time when the molecule is seen from its minor axis considering an elliptical structure after unfolding. These findings point toward partial unfolding of the protein while adduct formation is occurring, followed by more unfolded states when the uptaken ions start clustering. This is seen experimentally for the first time, and this data seems to answer a long unanswered puzzle on how clusters form inside a protein cavity.

The different charge states of a protein can exhibit different types of conformers as reported for charge induced unfolding of the protein.[60−62] Mainly two forces are responsible for gas-phase conformations of the protein ions. The balance between attractive intramolecular interactions, intramolecular charge solvation, and coulomb repulsion decides the conformational change of proteins. For higher charge state of the protein ion, coulomb repulsion predominates the intramolecular interactions. To minimize the repulsion, unzipping of the protein structures take place. Considering these phenomena, different charge states will show different degrees of unfolding upon Au addition. To confirm this claim, +10, +11, +12, and +13 charge states before and after Au binding were compared in Figure 3.

To reduce complications, the effects of five Au attachments on +10, +11, +12, and +13 charge states are shown in Figure 3. The folded state of Lyz has a +10 charge state at maximum intensity and shows a proper Gaussian shape in its mobilogram. As discussed above, decreased or increased charge state of the same entity may have different conformers leading to multiple peaks in the mobilogram. Each of these conformers upon Au addition will have more conformers with a slight change in their size and shape. This will lead to the broadening of the overall mobilogram, as all of the conformers cannot be separated from the larger envelope. The degree of broadening and number of conformers are highly depended on the charge state. This is reflected for five Au attachments to Lyz where +10, +11, +12, and +13 charge states showed a completely different degree of unfolding resulting in different CCS values. In the process of ion mobility separation, the ions are subjected to collide with N_2 gas. The effective area for the interaction between the individual ion and the neutral gas through which it is traveling is the measure of the collision cross section of the ions. From the CCS value, the structurally different conformers can be isolated in the gas phase. The unfolded structure will show more CCS value than the folded one as a result of different cross section values while colliding with N_2 gas. Here the Au attachment to protein increased the CCS value more than the native protein. Each of the CCS values was calculated separately and plotted against the number of Au attachments to the protein for a specific charge state (Figure 3E), which follows an almost linear relationship, confirming stepwise unfolding of the protein upon Au addition.

Collision-induced unfolding (CIU)[41,63] is a technique to understand the change of a native protein after forming a complex in ion mobility mass spectrometry through fragmentation of a specific charge state by collision/surface induced dissociation (CID/SID). A specific charge state is normally

DOI: 10.1021/acs.jpcc.7b02436
J. Phys. Chem. C 2017, 121, 13335−13344

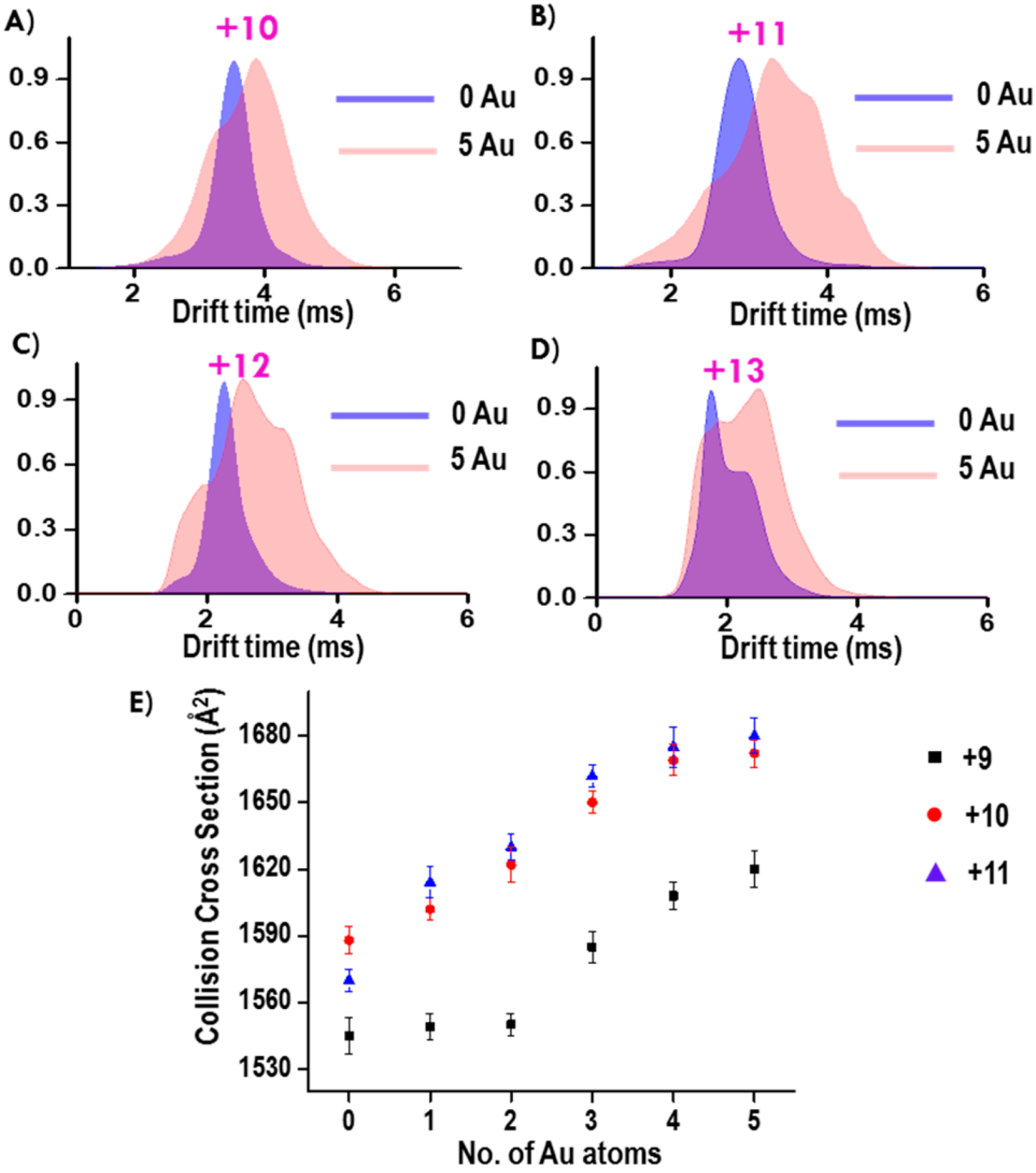

Figure 3. Ion mobility drift time of different charge states. The degree of unfolding depends highly on the charge state: +10 (A), +11 (B), +12 (C), +13 (D) represent different charge states of protein and Au_n-protein adduct. (E) Collision cross sections (CCS) calculated from the ion mobility MS data show increasing unfolding (higher ccs value) with higher numbers of Au attachment.

selected, and the fragmentation is monitored at different collision energies. The same charge state of the protein adduct is also studied in a similar way and compared with the native protein. The relative changes in the protein structure are analyzed by this method, which is an established way to understand protein unfolding/folding in the gas phase. If the minimal collision energy required to fragment the adduct is more than the native protein, the adduct is more stable than its native form and vice versa. Most of the proteins try to attain a folded state if not get modified and require more energy to fragment. During adduct formation, unfolding occurs and the protein becomes more susceptible to fragmentation at the same condition. This, in turn, validates the relative stability of the two. This phenomenon was studied in detail for Lyz and the Au_n-Lyz system, and the data are represented in Figure 4. The CIU plot for Lyz at its +10 charge state is shown in Figure 4A which, although exhibits successive fragmentation at higher collision energy, the parent protein peak was more intense than the fragments, even at a CE of 80 V (laboratory collision energy). Partial unfolding of the protein upon formation of Au_n-Lyz was evident from the broadness of the mobilogram as well as from the higher CCS value. Moreover, Au_2-Lyz showed a higher tendency for fragmentation and was not present beyond a CE of 60 V (Figure 4B). As more unfolded state is prone to higher fragmentation, Au_n-Lyz was less stable than the parent protein when compared to the same charge state. This study confirms a lesser stability of the protein upon Au attachment and a higher tendency to fragmentation, which in turn confirms the unfolding of the protein after Au binding. The corresponding CID data were given in Figure S2. A similar observation was found while cluster formations occurred where more protein fragments were found.[39] This conjecture again

DOI: 10.1021/acs.jpcc.7b02436
J. Phys. Chem. C 2017, 121, 13335−13344

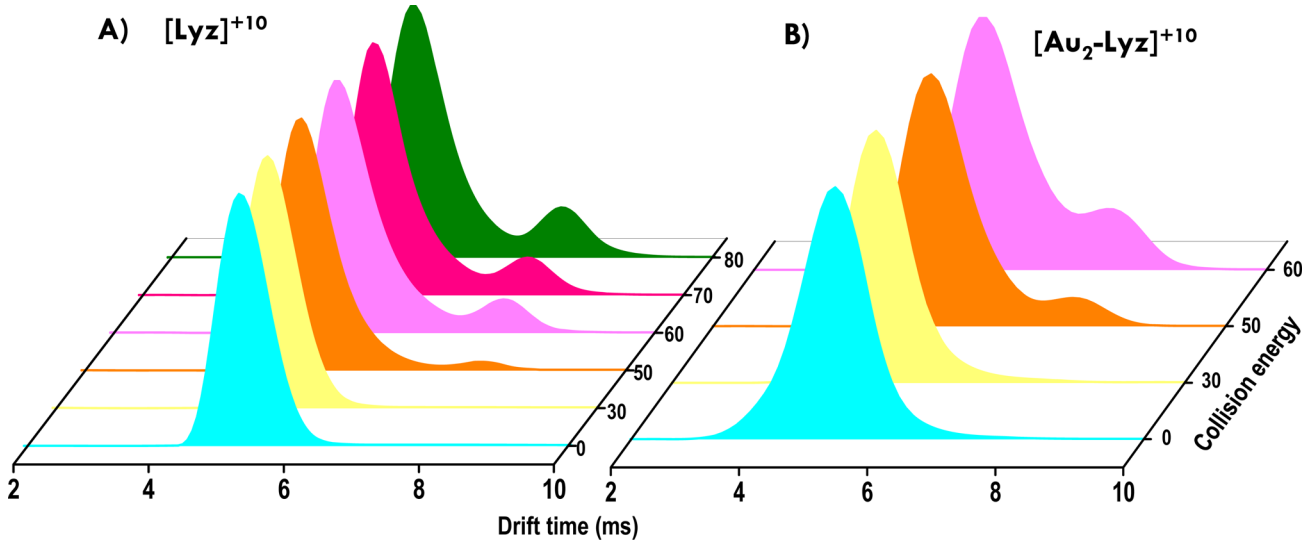

Figure 4. (A) Ion mobility drift time of Lyz at different collision energy showing unfolding of the protein at higher collision energy. (B) Au_n-Lyz adduct at different collision energy showing more unfolding and more prone toward fragmentation.

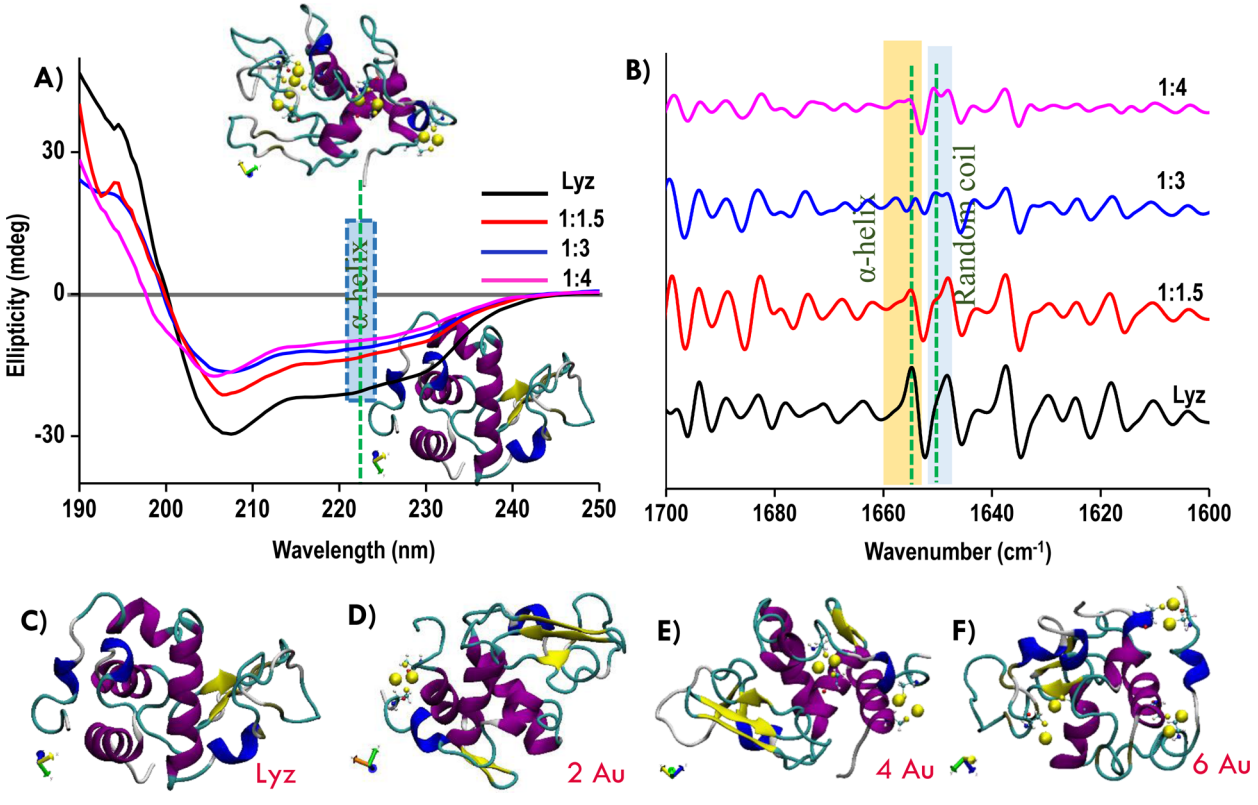

Figure 5. (A) CD spectra of the Lyz and Au_n-Lyz complex at different Au/Lyz ratios like 1:1.5, 1:3, and 1:4. (B) Second derivative of FTIR spectra of Au attached Lyz in these ratios. (C), (D), (E), (F) are the simulated structures of the Lyz and Au_n-Lyz complexes of 2, 4, and 6 Au. Condensed phase results are well matched with the simulated ones.

presents the need to understand the change in protein structure and a detailed mechanistic pathway of protein unfolding during cluster formation.

To understand the unfolding in solution and compare the findings that obtained from gas phase studies, CD and IR were studied in detail. Helicity of a protein can be directly measured from its CD spectrum.[18] With the increase in Au^{3+} concentration compared to protein, a gradual decrease in %α-helix was observed, as the peak at 222 nm becomes more shallow when more Au^{3+} is added. More than half of the helicity disappeared at the maximum Au^{3+} concentration. This data clearly prove solution state unfolding of the protein upon Au addition (see Figure 5A).

This conformational relaxation of protein after Au^{3+} addition was characterized by FTIR spectroscopy also.[18,25,64] The change in the protein's secondary structure is reflected in the amide region, amide bands I (1600−1690 cm^{-1}), II (1480−1575 cm^{-1}), III (1229−1301 cm^{-1}), and amide A (3300 cm^{-1}).

DOI: 10.1021/acs.jpcc.7b02436
J. Phys. Chem. C 2017, 121, 13335−13344

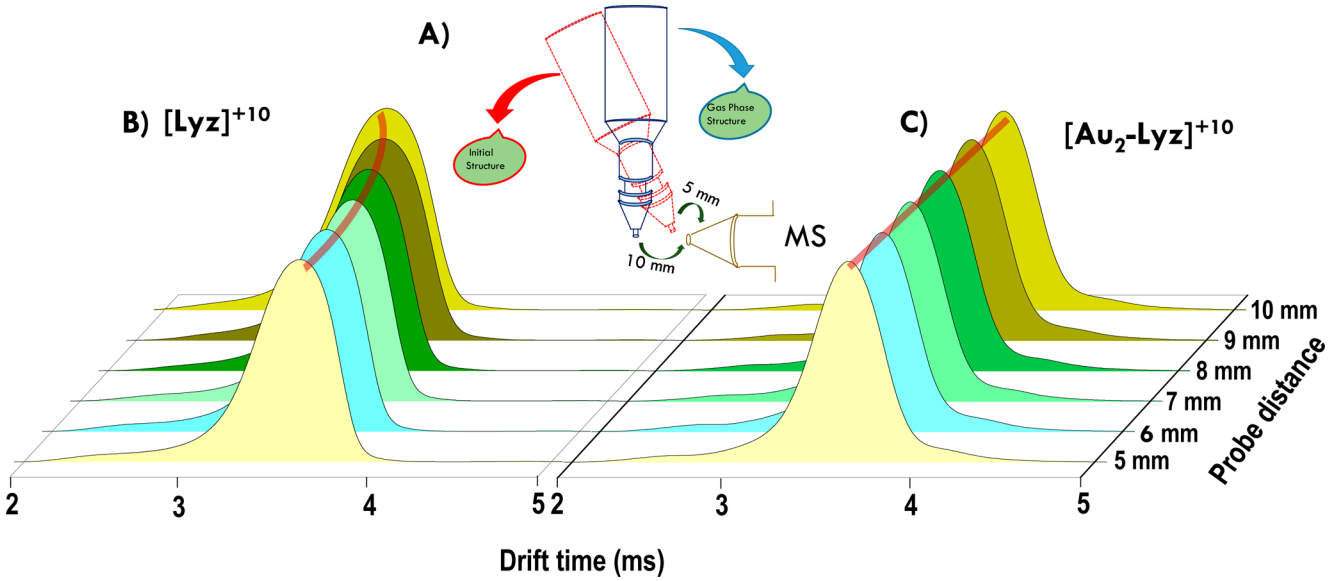

Figure 6. Probe distance-dependent study of protein and complex. (A) Schematic of different probe distance in MS. (B) and (C) are the structural changes for Lyz and Au attached Lyz, respectively.

The band near 1650 cm^{-1}, a signature of amide I, appears from the contribution of C═O stretching vibration and out of plane C−N stretching. The change of N−H bending in the structures is attributed to the Amide II regions. A broad band near 3300−3000 cm^{-1} in the amide A region can be assigned due to N−H and O−H stretching vibrations. The second derivative of IR (in the region 1600−1700 cm^{-1}) is more sensitive toward the changes in the amide region during Au_n-Lyz formation. A large change in the α-helix region among all the changes of secondary structures like α-helix (1651−1658 cm^{-1}), β-sheets (1618−1642 cm^{-1}), random coils (1640−1650 cm^{-1}), and turns (1666−1688 cm^{-1}) was clear from Figure 5. The band around 1654 cm^{-1} was found to become featureless at higher Au ion concentration, which supports the earlier IR data reported for Au@Lyz.[18] Due to the huge perturbation in the α-helical region, the protein structure became relaxed which supports our gas phase data also. The full range IR spectra of Lyz and Au_n-Lyz complexes are shown in Figure S3 and the amide band I region (1600−1690 cm^{-1}) of each spectra are shown along with their second derivatives in Figure S4.

Experiments have shown that gold ions bind to proteins through the formation of Au−S bonds with cysteine.[18,36] In Lyz, free cysteine residues are not available, as they are involved in disulfide bonds. The secondary structural units hold together with the help of four disulfide bonds. Gold ions were covalently attached to cysteine by breaking the disulfide bonds. For each cystine, two Au^+ were added in order to understand the structural changes in Lyz after complexation with Au^+. First, two gold ions were added to the disulfide bond (Cys127 and Cys6), which were present on the outer surface of Lyz. Then 4 (2 two disulfide bonds), 6 (3 disulfide bonds), and 8 (4 disulfide bonds) gold ions were attached to Lyz through Au−S bond formation. Molecular dynamics simulations have been carried out for all the complexes of gold ions and Lyz. The snapshots of the simulated structures were shown in Figure 5C−F. It may be noted from Figure 5C−F that variations occur in the secondary structure of Lyz. The enlarged snapshots of all the simulated structures are shown in Figures S5−S9. The calculated residue-wise secondary structures for all the complexes are shown in Figures S11 and S12 and the same for native Lyz is presented in Figure S10. It can be observed that the residues (98−114) underwent slight changes in their conformation after addition of two gold ions. The deviations in the α-helical structural units of Lyz increased with the increase in the number of gold ions. The calculated helical content of Lyz is 40, 36, 34, 34, and 28% in the case of native Lyz, Au_2-Lyz, Au_4-Lyz, Au_6-Lyz, and Au_8-Lyz, respectively. In all the cases, α-helical conformation adopts the turn form after Lyz bind to Au^+. The changes in α-helicity calculated from the CD spectra corroborate well with the values obtained from MD simulations.

Conditions used in electrospray ionization are known to have definite effects on the structure of the analyte species.[65,66] Changes in relative abundances of isomers were observed during ionization for small molecules such as peptides, carbohydrates etc. In a very recent report, Xia et al. have shown[67] that changing the probe position, desolvation temperature, capillary voltage, sample infusion flow rate and cone voltage, the relative population of the tautomer can be changed in the case of p-hydroxybenzoic acid. When the probe tip is close to the cone aperture, that is, under high field conditions, ions can preserve their solution based ionic structures. But when the distance between the spray needle and the entrance orifice is more, that is, under low field condition, gas phase ion population is enhanced. This phenomenon can be justified by charge ion evaporation and charge residue models. For macromolecules like proteins, the structure shrinks in the gas phase due to dehydration.[68] In the solvent-free environment, the structures turn "inside out", that is, the hydrophobic part comes out and the polar segment moves inward.[58]

If a protein is unfolded in the solution before ESI, it will not show any change with varying probe distance. But if the unfolding is a purely gas phase phenomenon, there will be a significant change with decrease or increase in probe distance. To illustrate the structural changes of the protein due to the Au attachment, a probe distance dependent ESI IM-MS study was performed for both native protein and its Au-adduct. The native protein showed substantial changes while changing the probe distance, confirming shrinkage in the gas phase

DOI: 10.1021/acs.jpcc.7b02436
J. Phys. Chem. C 2017, 121, 13335−13344

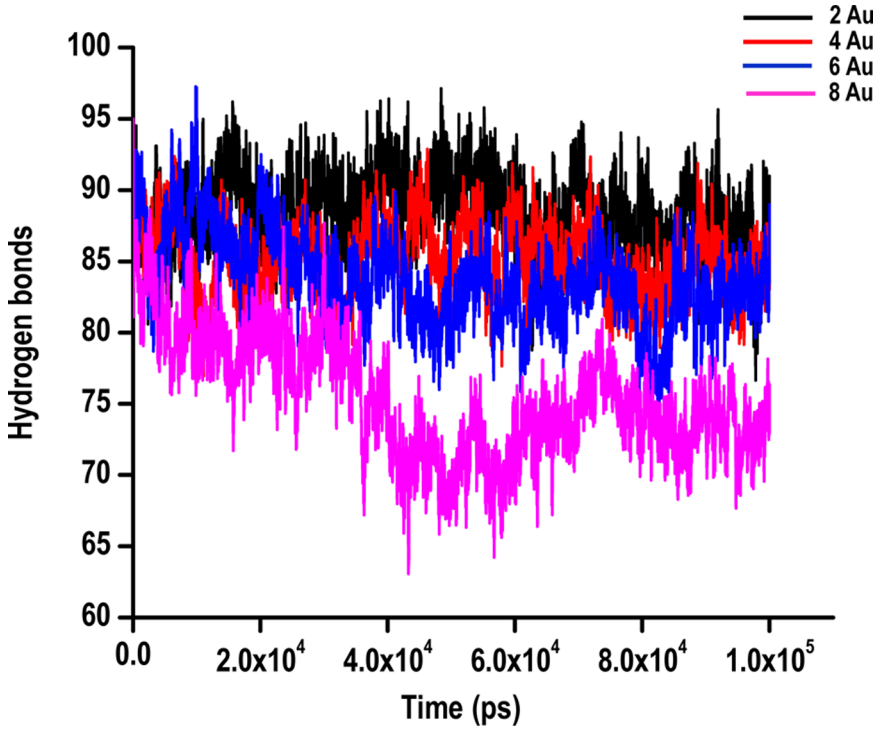

Figure 7. Simulated data of breaking of H-bonds with time for 2, 4, 6, and 8 Au attached protein, showing more Au attachment leads to uncoiling of the protein structure.

compared to condensed phase when the probe distance was varied from 5 to 10 mm (see Figure 6B). As the probe distance was increased, the protein was exposed to the gaseous state for more time. Consequently, the structures became more compact and the drift times shifted to lower values.

This kind of change in the drift time, however, was not observed for the Au_n-Lyz with varying probe distances (Figure 6C). These suggest that the Au-induced unfolding of Lyz has already happened in the solution state. Shrinkage of these unfolded species does not happen effectively during the electrospray ionization process, resulting in similar drift time.

To prove such fluctuation in the protein structures upon Au binding, we have calculated the root-mean-square fluctuation (RMSF) and conformational entropy for Lyz and Au_n-Lyz. The calculated RMSF for Lyz in the case of native Lyz and Au_8-Lyz are presented in Figure S13. The fluctuation of residues is suppressed slightly upon binding with Au^+ ions except for the residues from 40 to 60. The decrease in the flexibility of Lyz is marginal in the presence of gold ions when compared to native Lyz. Conformational entropy values were calculated using principal component analysis which was performed on the trajectories of native Lyz and Au_8-Lyz. The calculated conformational entropy values for Lyz are 2.45 and 2.21 kJ mol^{-1} K in the case of native Lyz and Au_8-Lyz, respectively. The less conformational entropy in the case of Au_8-Lyz indicates more rigidity of Lyz in the adduct than in the native state.The secondary structural elements present in Lyz are α-helix, antiparallel β sheet, long loop, and a 3_{10} helix. These structural units are stabilized with the formation of the hydrogen bonds between the residues. The calculated number of hydrogen bonds is presented in Figure 7. It can be clearly seen that a decrease in a number of hydrogen bonds occurs with an increase in simulation time. The average number of hydrogen bonds of Lyz in the case of $2Au^+$, $4Au^+$, $6Au^+$, and $8Au^+$ addition are 88, 85, 84, and 75, respectively. The reduction in hydrogen bonds increases with the increase in a number of Au^+. Overall, the results affirm the unfolding of secondary structural elements of Lyz upon binding with Au^+.

SUMMARY AND CONCLUSIONS

A comparison between gas phase and solution phase studies of Lyz and Au_n-Lyz demonstrated the structural changes of protein during Au@Lyz formation. Gas phase conformers observed for different charge states of native protein as well as Au_n-Lyz were separated by ion mobility mass spectrometry. Change in their collision cross section upon Au binding showed qualitative unfolding of the protein. The unfolding was indeed a solution phase phenomenon and such conformers were retained in the gas phase. A detailed understanding of the protein's conformational change was performed by MD simulations, which supported the experimental observation in the gaseous and condensed phases. This study would help to understand the exact mechanism of formation of protein protected clusters and can explain a few puzzles related to the formation event. The difference between the CCS of the native protein and after cluster formation may allow us to estimate the cluster size and structural changes of the protein simultaneously.

ASSOCIATED CONTENT

Supporting Information

The Supporting Information is available free of charge on the ACS Publications website at DOI: 10.1021/acs.jpcc.7b02436.

The structure of Lyz, residue-wise calculated secondary structure of Lyz and Au_n-Lyz, MS/MS studies of Lyz and Au2-Lyz, simulated structures of Au_n-Lyz, RMSF of Lyz and Au_8-Lyz, IR spectra of Lyz and Au_n-Lyz (PDF).

DOI: 10.1021/acs.jpcc.7b02436
J. Phys. Chem. C 2017, 121, 13335−13344

AUTHOR INFORMATION

Corresponding Author

*E-mail: pradeep@iitm.ac.in.

ORCID

Venkatesan Subramanian: 0000-0003-2463-545X

Thalappil Pradeep: 0000-0003-3174-534X

Present Address

§Presently a postdoctoral fellow at Karlsruhe Institute of Technology (KIT), Institute of Nanotechnology, Hermannvon-Helmholtz-Platz 1, 76344 Eggenstein-Leopoldshafen, Germany.

Author Contributions

‡D.G. and A.B. contributed equally to this work.

Notes

The authors declare no competing financial interest.

ACKNOWLEDGMENTS

We thank the Department of Science and Technology, Government of India, for continuous support of our research program on nanomaterials. D.G and A.N. thank IIT Madras for student fellowships.

REFERENCES

(1) Mathew, A.; Pradeep, T. Noble Metal Clusters: Applications in Energy, Environment, and Biology. *Part. Part. Syst. Charact.* **2014**, *31*, 1017−1053.

(2) Udayabhaskararao, T.; Pradeep, T. New Protocols for the Synthesis of Stable Ag and Au Nanocluster Molecules. *J. Phys. Chem. Lett.* **2013**, *4*, 1553−1564.

(3) Jin, R.; Zeng, C.; Zhou, M.; Chen, Y. Atomically Precise Colloidal Metal Nanoclusters and Nanoparticles: Fundamentals and Opportunities. *Chem. Rev.* **2016**, *116*, 10346−10413.

(4) Jin, R. Atomically Precise Metal Nanoclusters: Stable Sizes and Optical Properties. *Nanoscale* **2015**, *7*, 1549−1565.

(5) Zheng, J.; Nicovich, P. R.; Dickson, R. M. Highly Fluorescent Noble-Metal Quantum Dots. *Annu. Rev. Phys. Chem.* **2007**, *58*, 409−431.

(6) Hassinen, J.; Pulkkinen, P.; Kalenius, E.; Pradeep, T.; Tenhu, H.; Hakkinen, H.; Ras, R. H. A. Mixed-Monolayer-Protected Au25 Clusters with Bulky Calix[4]Arene Functionalities. *J. Phys. Chem. Lett.* **2014**, *5*, 585−589.

(7) Petty, J. T.; Story, S. P.; Hsiang, J.-C.; Dickson, R. M. DNA-Templated Molecular Silver Fluorophores. *J. Phys. Chem. Lett.* **2013**, *4*, 1148−1155.

(8) Baral, A.; Basu, K.; Ghosh, S.; Bhattacharyya, K.; Roy, S.; Datta, A.; Banerjee, A. Size Specific Emission in Peptide Capped Gold Quantum Clusters with Tunable Photoswitching Behavior. *Nanoscale* **2017**, *9*, 4419−4429.

(9) Liu, X.; Ding, W.; Wu, Y.; Zeng, C.; Luo, Z.; Fu, H. Penicillamine-Protected Ag_{20} Nanoclusters and Fluorescence Chemosensing for Trace Detection of Copper Ions. *Nanoscale* **2017**, *9*, 3986−3994.

(10) Li, G.; Abroshan, H.; Liu, C.; Zhuo, S.; Li, Z.; Xie, Y.; Kim, H. J.; Rosi, N. L.; Jin, R. Tailoring the Electronic and Catalytic Properties of Au25 Nanoclusters Via Ligand Engineering. *ACS Nano* **2016**, *10*, 7998−8005.

(11) Hu, D.; Sheng, Z.; Gong, P.; Zhang, P.; Cai, L. Highly Selective Fluorescent Sensors for Hg2+ Based on Bovine Serum Albumin-Capped Gold Nanoclusters. *Analyst* **2010**, *135*, 1411−1416.

(12) Wei, H.; Wang, Z.; Yang, L.; Tian, S.; Hou, C.; Lu, Y. Lysozyme-Stabilized Gold Fluorescent Cluster: Synthesis and Application as Hg2+ Sensor. *Analyst* **2010**, *135*, 1406−1410.

(13) Wei, H.; et al. Time-Dependent, Protein-Directed Growth of Gold Nanoparticles within a Single Crystal of Lysozyme. *Nat. Nanotechnol.* **2011**, *6*, 93−97.

(14) Liang, M.; Wang, L.; Liu, X.; Qi, W.; Su, R.; Huang, R.; Yu, Y.; He, Z. Cross-Linked Lysozyme Crystal Templated Synthesis of Au Nanoparticles as High-Performance Recyclable Catalysts. *Nanotechnology* **2013**, *24*, 245601−245608.

(15) Wei, H.; Lu, Y. Catalysis of Gold Nanoparticles within Lysozyme Single Crystals. *Chem. - Asian J.* **2012**, *7*, 680−683.

(16) Yang, T.; Li, Z.; Wang, L.; Guo, C.; Sun, Y. Synthesis, Characterization, and Self-Assembly of Protein Lysozyme Monolayer-Stabilized Gold Nanoparticles. *Langmuir* **2007**, *23*, 10533−10538.

(17) Lin, Y.-H.; Tseng, W.-L. Ultrasensitive Sensing of Hg2+ and Ch3hg+ Based on the Fluorescence Quenching of Lysozyme Type Vi-Stabilized Gold Nanoclusters. *Anal. Chem.* **2010**, *82*, 9194−9200.

(18) Baksi, A.; Xavier, P. L.; Chaudhari, K.; Goswami, N.; Pal, S. K.; Pradeep, T. Protein-Encapsulated Gold Cluster Aggregates: The Case of Lysozyme. *Nanoscale* **2013**, *5*, 2009−2016.

(19) Baksi, A.; Pradeep, T. Noble Metal Alloy Clusters in the Gas Phase Derived from Protein Templates: Unusual Recognition of Palladium by Gold. *Nanoscale* **2013**, *5*, 12245−12254.

(20) Baksi, A.; Pradeep, T.; Yoon, B.; Yannouleas, C.; Landman, U. Bare Clusters Derived from Protein Templates: Au25+, Au38+ and Au102+. *ChemPhysChem* **2013**, *14*, 1272−1282.

(21) Mathew, A.; Sajanlal, P. R.; Pradeep, T. A Fifteen Atom Silver Cluster Confined in Bovine Serum Albumin. *J. Mater. Chem.* **2011**, *21*, 11205−11212.

(22) Mohanty, J. S.; Baksi, A.; Lee, H.; Pradeep, T. Noble Metal Clusters Protected with Mixed Proteins Exhibit Intense Photoluminescence. *RSC Adv.* **2015**, *5*, 48039−48045.

(23) Chaudhari, K.; Pradeep, T. Initial Growth Kinetics of Luminescent Quantum Clusters of Silver within Albumin Family Protein Templates. *J. Phys. Chem. C* **2015**, *119*, 9988−9994.

(24) Chaudhari, K.; Xavier, P. L.; Predeep, T. Understanding the Evolution of Luminescent Gold Quantum Clusters in Protein Templates. *ACS Nano* **2011**, *5*, 8816−8827.

(25) Xavier, P. L.; Chaudhari, K.; Verma, P. K.; Pal, S. K.; Pradeep, T. Luminescent Quantum Clusters of Gold in Transferrin Family Protein, Lactoferrin Exhibiting Fret. *Nanoscale* **2010**, *2*, 2769−2776.

(26) Mohanty, J. S.; Xavier, P. L.; Chaudhari, K.; Bootharaju, M. S.; Goswami, N.; Pal, S. K.; Pradeep, T. Luminescent, Bimetallic Auag Alloy Quantum Clusters in Protein Templates. *Nanoscale* **2012**, *4*, 4255−4262.

(27) Xie, J.; Zheng, Y.; Ying, J. Y. Highly Selective and Ultrasensitive Detection of Hg2+ Based on Fluorescence Quenching of Au Nanoclusters by Hg2+-Au+ Interactions. *Chem. Commun.* **2010**, *46*, 961−963.

(28) Goswami, N.; Zheng, K.; Xie, J. Bio-Ncs - the Marriage of Ultrasmall Metal Nanoclusters with Biomolecules. *Nanoscale* **2014**, *6*, 13328−13347.

(29) Song, X.-R.; Goswami, N.; Yang, H.-H.; Xie, J. Functionalization of Metal Nanoclusters for Biomedical Applications. *Analyst* **2016**, *141*, 3126−3140.

(30) Wang, Y.; Chen, J.; Irudayaraj, J. Nuclear Targeting Dynamics of Gold Nanoclusters for Enhanced Therapy of Her2+ Breast Cancer. *ACS Nano* **2011**, *5*, 9718−9725.

(31) Yu, Y.; New, S. Y.; Xie, J.; Su, X.; Tan, Y. N. Protein-Based Fluorescent Metal Nanoclusters for Small Molecular Drug Screening. *Chem. Commun.* **2014**, *50*, 13805−13808.

(32) Zhou, W.; Cao, Y.; Sui, D.; Guan, W.; Lu, C.; Xie, J. Ultrastable Bsa-Capped Gold Nanoclusters with a Polymer-Like Shielding Layer against Reactive Oxygen Species in Living Cells. *Nanoscale* **2016**, *8*, 9614−9620.

(33) Zhang, A.; Tu, Y.; Qin, S.; Li, Y.; Zhou, J.; Chen, N.; Lu, Q.; Zhang, B. Gold Nanoclusters as Contrast Agents for Fluorescent and X-Ray Dual-Modality Imaging. *J. Colloid Interface Sci.* **2012**, *372*, 239−244.

(34) Wu, X.; He, X.; Wang, K.; Xie, C.; Zhou, B.; Qing, Z. Ultrasmall near-Infrared Gold Nanoclusters for Tumor Fluorescence Imaging in Vivo. *Nanoscale* **2010**, *2*, 2244−2249.

DOI: 10.1021/acs.jpcc.7b02436
J. Phys. Chem. C 2017, 121, 13335−13344

(35) Zhang, X.-D.; et al. Enhanced Tumor Accumulation of Sub-2 Nm Gold Nanoclusters for Cancer Radiation Therapy. *Adv. Healthcare Mater.* **2014**, *3*, 133−141.
(36) Xavier, P. L.; Chaudhari, K.; Baksi, A.; Pradeep, T. Protein-Protected Luminescent Noble Metal Quantum Clusters: An Emerging Trend in Atomic Cluster Nanoscience. *Nano Rev.* **2012**, *3*, 14767.
(37) Habeeb Muhammed, M. A.; Verma, P. K.; Pal, S. K.; Retnakumari, A.; Koyakutty, M.; Nair, S.; Pradeep, T. Luminescent Quantum Clusters of Gold in Bulk by Albumin-Induced Core Etching of Nanoparticles: Metal Ion Sensing, Metal-Enhanced Luminescence, and Biolabeling. *Chem. - Eur. J.* **2010**, *16* (33), 10103−10112.
(38) Lin, C.-A. J.; et al. Synthesis, Characterization, and Bioconjugation of Fluorescent Gold Nanoclusters toward Biological Labeling Applications. *ACS Nano* **2009**, *3*, 395−401.
(39) Baksi, A.; Mitra, A.; Mohanty, J. S.; Lee, H.; De, G.; Pradeep, T. Size Evolution of Protein-Protected Gold Clusters in Solution: A Combined Saxs-Ms Investigation. *J. Phys. Chem. C* **2015**, *119*, 2148−2157.
(40) Wyttenbach, T.; Grabenauer, M.; Thalassinos, K.; Scrivens, J. H.; Bowers, M. T. The Effect of Calcium Ions and Peptide Ligands on the Relative Stabilities of the Calmodulin Dumbbell and Compact Structures. *J. Phys. Chem. B* **2010**, *114*, 437−447.
(41) Bartman, C. E.; Metwally, H.; Konermann, L. Effects of Multidentate Metal Interactions on the Structure of Collisionally Activated Proteins: Insights from Ion Mobility Spectrometry and Molecular Dynamics Simulations. *Anal. Chem.* **2016**, *88*, 6905−6913.
(42) Flick, T. G.; Merenbloom, S. I.; Williams, E. R. Effects of Metal Ion Adduction on the Gas-Phase Conformations of Protein Ions. *J. Am. Soc. Mass Spectrom.* **2013**, *24*, 1654−1662.
(43) Artymiuk, P. J.; Blake, C. C. F.; Rice, D. W.; Wilson, K. S. The Structures of the Monoclinic and Orthorhombic Forms of Hen Egg-White Lysozyme at 6 Å Resolution. *Acta Crystallogr., Sect. B: Struct. Crystallogr. Cryst. Chem.* **1982**, *38*, 778−783.
(44) Cornell, W. D.; Cieplak, P.; Bayly, C. I.; Gould, I. R.; Merz, K. M., Jr.; Ferguson, D. M.; Spellmeyer, D. C.; Fox, T.; Caldwell, J. W.; Kollman, P. A. A Second Generation Force Field for the Simulation of Proteins, Nucleic Acids, and Organic Molecules. *J. Am. Chem. Soc.* **1995**, *117*, 5179−97.
(45) Mudedla, S. K.; Singam, E. R. A.; Vijay Sundar, J.; Pedersen, M. N.; Murugan, N. A.; Kongsted, J.; Agren, H.; Subramanian, V. Enhancement of Internal Motions of Lysozyme through Interaction with Gold Nanoclusters and Its Optical Imaging. *J. Phys. Chem. C* **2015**, *119*, 653−664.
(46) Mudedla, S. K.; Azhagiya Singam, E. R.; Balamurugan, K.; Subramanian, V. Influence of the Size and Charge of Gold Nanoclusters on Complexation with Sirna: A Molecular Dynamics Simulation Study. *Phys. Chem. Chem. Phys.* **2015**, *17*, 30307−30317.
(47) Nose, S.; Klein, M. L. Constant Pressure Molecular Dynamics for Molecular Systems. *Mol. Phys.* **1983**, *50*, 1055−76.
(48) Parrinello, M.; Rahman, A. Polymorphic Transitions in Single Crystals: A New Molecular Dynamics Method. *J. Appl. Phys.* **1981**, *52*, 7182−90.
(49) Bussi, G.; Donadio, D.; Parrinello, M. Canonical Sampling through Velocity Rescaling. *J. Chem. Phys.* **2007**, *126*, 014101/1−014101/7.
(50) Berendsen, H. J. C.; van der Spoel, D.; van Drunen, R. Gromacs: A Message-Passing Parallel Molecular Dynamics Implementation. *Comput. Phys. Commun.* **1995**, *91*, 43−56.
(51) Lindahl, E.; Hess, B.; van der Spoel, D. Gromacs 3.0: A Package for Molecular Simulation and Trajectory Analysis. *J. Mol. Model.* **2001**, *7*, 306−317.
(52) Hess, B.; Kutzner, C.; van der Spoel, D.; Lindahl, E. Gromacs 4: Algorithms for Highly Efficient, Load-Balanced, and Scalable Molecular Simulation. *J. Chem. Theory Comput.* **2008**, *4*, 435−447.
(53) Essmann, U.; Perera, L.; Berkowitz, M. L.; Darden, T.; Lee, H.; Pedersen, L. G. A Smooth Particle Mesh Ewald Method. *J. Chem. Phys.* **1995**, *103*, 8577−93.
(54) Hess, B.; Bekker, H.; Berendsen, H. J. C.; Fraaije, J. G. E. M. Lincs: A Linear Constraint Solver for Molecular Simulations. *J. Comput. Chem.* **1997**, *18*, 1463−1472.
(55) Humphrey, W.; Dalke, A.; Schulten, K. Vdm: Visual Molecular Dynamics. *J. Mol. Graphics* **1996**, *14*, 33−8.
(56) Angel, L. A. Study of Metal Ion Labeling of the Conformational and Charge States of Lysozyme by Ion Mobility Mass Spectrometry. *Eur. Mass Spectrom.* **2011**, *17*, 207−215.
(57) Valentine, S. J.; Anderson, J. G.; Ellington, A. D.; Clemmer, D. E. Disulfide-Intact and -Reduced Lysozyme in the Gas Phase: Conformations and Pathways of Folding and Unfolding. *J. Phys. Chem. B* **1997**, *101*, 3891−3900.
(58) Lanucara, F.; Holman, S. W.; Gray, C. J.; Eyers, C. E. The Power of Ion Mobility-Mass Spectrometry for Structural Characterization and the Study of Conformational Dynamics. *Nat. Chem.* **2014**, *6*, 281−294.
(59) Ruotolo, B. T.; Benesch, J. L. P.; Sandercock, A. M.; Hyung, S.-J.; Robinson, C. V. Ion Mobility-Mass Spectrometry Analysis of Large Protein Complexes. *Nat. Protoc.* **2008**, *3*, 1139−1152.
(60) Mao, Y.; Ratner, M. A.; Jarrold, M. F. Molecular Dynamics Simulations of the Charge-Induced Unfolding and Refolding of Unsolvated Cytochrome C. *J. Phys. Chem. B* **1999**, *103*, 10017−10021.
(61) Gonzalez Florez, A. I.; Mucha, E.; Ahn, D.-S.; Gewinner, S.; Schoellkopf, W.; Pagel, K.; von Helden, G. Charge-Induced Unzipping of Isolated Proteins to a Defined Secondary Structure. *Angew. Chem., Int. Ed.* **2016**, *55*, 3295−3299.
(62) Shelimov, K. B.; Clemmer, D. E.; Hudgins, R. R.; Jarrold, M. F. Protein Structure in Vacuo: Gas-Phase Conformations of Bpti and Cytochrome C. *J. Am. Chem. Soc.* **1997**, *119*, 2240−2248.
(63) Hopper, J. T. S.; Oldham, N. J. Collision Induced Unfolding of Protein Ions in the Gas Phase Studied by Ion Mobility-Mass Spectrometry: The Effect of Ligand Binding on Conformational Stability. *J. Am. Soc. Mass Spectrom.* **2009**, *20*, 1851−1858.
(64) Zhang, M.; Dang, Y.-Q.; Liu, T.-Y.; Li, H.-W.; Wu, Y.; Li, Q.; Wang, K.; Zou, B. Pressure-Induced Fluorescence Enhancement of the Bsa-Protected Gold Nanoclusters and the Corresponding Conformational Changes of Protein. *J. Phys. Chem. C* **2013**, *117*, 639−647.
(65) Tian, Z.; Kass, S. R. Does Electrospray Ionization Produce Gas-Phase or Liquid-Phase Structures? *J. Am. Chem. Soc.* **2008**, *130*, 10842−10843.
(66) Schroder, D.; Budesinsky, M.; Roithova, J. Deprotonation of P-Hydroxybenzoic Acid: Does Electrospray Ionization Sample Solution or Gas-Phase Structures? *J. Am. Chem. Soc.* **2012**, *134*, 15897−15905.
(67) Xia, H.; Attygalle, A. B. Effect of Electrospray Ionization Source Conditions on the Tautomer Distribution of Deprotonated P-Hydroxybenzoic Acid in the Gas Phase. *Anal. Chem.* **2016**, *88*, 6035−6043.
(68) Chen, S.-H.; Chen, L.; Russell, D. H. Metal-Induced Conformational Changes of Human Metallothionein-2a: A Combined Theoretical and Experimental Study of Metal-Free and Partially Metalated Intermediates. *J. Am. Chem. Soc.* **2014**, *136*, 9499−9508.

DOI: 10.1021/acs.jpcc.7b02436
J. Phys. Chem. C 2017, 121, 13335−13344